Atmósfera 16 (2003) 67–82

Diagnostic study on the relation between ozone and potential vorticity

H. ABDEL BASSET [a] and A. GAHEIN [b]

[a] *Department of Astronomy and Meteorology, Faculty of Science, Al-Azhar University, Cairo, Egypt, Nasr City, Cairo, Egypt, email: h.abdelbasset@excite.com*

[b] *Egyptian Meteorological Authority, Cairo, Egypt*

Received June 12, 2001; accepted June 20, 2002

RESUMEN

Se presenta un análisis diagnóstico de un sistema mediterráneo y del pliegue de la tropopausa asociado durante el periodo del 27 de febrero al 10 de marzo de 1987. Se diagnosticaron la altitud geopotencial, el potencial de vorticidad y la distribución de la humedad relativa. El análisis indica una correlación clara entre el desarrollo de la baja segregada y el pliegue de la tropopausa. Una serie de cortes verticales en los extremos de las trazas del chorro demostraron que el pliegue puede ser capturado utilizando el potencial de vorticidad y la humedad relativa. Para investigar la movilidad vertical en la vecindad del pliegue se utilizaron vectores Q, y se demostraron las posiciones exactas de descenso correspondientes al pliegue a lo largo de toda la longitud de la traza del chorro. El análisis también mostró que la fuerte correlación entre el ozono total y la columna integrada del potencial de vorticidad es válida para todos los niveles. Como ambas cantidades son integrales a través de la atmósfera, este resultado es consistente con una dependencia lineal altamente independiente entre el ozono y el potencial de vorticidad, aunque no la prueba. Se necesitan más estudios de caso para asegurar la elevada dependencia lineal entre el ozono y el potencial de vorticidad. El transporte máximo de ozono de la estratosfera a la troposfera coincide con el desarrollo máximo del sistema y también con los valores máximos del potencial de vorticidad.

ABSTRACT

A diagnostic analysis of a Mediterranean system and the associated tropopause folding for the period 27 February to 10 March, 1987 is presented. Geopotential height, potential vorticity (PV) and relative humidity distributions were diagnosed. The analysis indicates clear correlation between the development of the cut-off low and the tropopause folding. A series of vertical cross-sections at the ends of the jet streaks demonstrated that a fold could be captured using potential vorticity and relative humidity. Q-vectors were employed to investigate vertical motion in the vicinity of the fold and showed the exact positions of descent corresponding to the fold along the entire length of the jet streak. The analysis also shows that the strong correlation between total ozone and column integrated potential vorticity holds well for all levels. As both quantities are integrals through the atmosphere this result is consistent with, but does not prove, a high independent linear dependence between ozone and PV. More case studies are needed to assure the high linear dependence between ozone and PV. The maximum transport of ozone from the stratosphere to the troposphere is coinciding with the maximum developing system, and also with the maximum values of PV.

Key words: Mediterranean, tropopause, ozone, potential vorticity

1. Introduction

Reed and Sanders (1953) discuss the idea of the description of fronts in terms of potential vorticity (PV). They show that using the PV-conservation theorem the frontal zone is a portion of the lower stratosphere that underwent strong subsidence with the tropopause. In Reed (1955), the PV conservation is used one step further by computing trajectories conserving PV. This enables the author to identify the origin of an air parcel and to clearly show that the intense portion of a frontal zone is composed of air of stratospheric origin. The study also indicates the importance of differential subsidence introducing upper-level frontogenesis and the associated tropopause fold in the northwesterly flow upstream of the trough axis. Hoskins and Bretherton (1972) first comprehensively treated tropopause folds within the framework of semi-geostrophic theory. With this concept the extratropical tropopause is dynamically defined by a threshold value of Ertel's potential vorticity rather than thermally. The air mass flux into the troposphere is driven by upper tropospheric frontogenesis that is mainly induced by a deformation flow field steepening horizontal temperature gradients at the tropopause height levels. Aircraft measurements of ozone, water vapor, cloud condensation nuclei, and their inter-comparison with PV (Shapiro, 1980; Browell *et al.*, 1987; Danielsen *et al.*, 1991) indicate that tropopause folds look as an isentropic down-gliding of stratospheric air masses as a branch of cross frontal secondary circulation at the frontogenetically active region. The dynamical tropopause appears as a fold with a length scale of the order of 100 km in the lateral direction and 1000 km in the longitudinal direction. From these scales it is obvious that the existence of a tropopause fold cannot be directly inferred from routine weather charts, whereas PV maps and satellite imagery of humidity can provide strong indications (Appenzeller and Davies, 1992; Appenzeller *et al.*, 1996). Since tropopause folds have been recognized as a main extratropical exchange mechanism using observational studies of folds have been conducted fairly extensively by various methods. A series of aircraft experiments (e.g., Danielsen, 1968; Danielsen and Mohnen, 1977; Danielsen *et al.*, 1991; Shapiro, 1980) focused on actual exchange rates of individual tropopause folds. Recently, LIDAR measurements by Ancellet *et al.* (1991, 1994) provided insight into the same quantity by ground-based instrumentation.

The present study considers the relation between total ozone and PV; the relation between tropopause folding with the polar jet was also part of the study.

1.1 Synoptic discussion

A case of winter cyclogenesis over the Mediterranean is considered. Its period includes the last 2 days of February and the first 10 days of March, 1987. Based on the surface charts, changes in the central of low and charts of 500 hPa, the life cycle of our cyclone can be divided as follows: the first 2 days (27-28 February) immediately preceding the onset of cyclogenesis can be termed as the precyclogenetic period. The period from 1- 6 March is the growth period, and finally the decay period extended from 7-10 March.

The cyclone of special interest first appeared as an extension of the crossing depression northern Europe at 0000 UTC on 27 February. By 28 February, the surface cyclone (not shown) moved slowly from south to southwestward as it deepened, and achieved its lowest central pressure of 1000 hPa at 0000 UTC on 3 March over northern Italy. Twenty-four hours later this low pressure intensified by more than 5 hPa and moved southeast to a point just south of Greece, associated with a cold cut-off low in the upper atmosphere. The 500 hPa trough (Figure 1) associated with the cyclone was well north of Europe by 0000 UTC on 28 February, a cut-off low at 500 hPa was centered over eastern Finland. A closed 500 hPa contour moved slowly southeastward on the second day of March (Figure 1). By 0000 UTC on 3 March, a drop in the contours of the 500 hPa level took place in conjunction with the deepening surface cyclone. It was also noticed that the horizontal extent of the 500 hPa trough became small and the geopotential trough lied behind the thermal trough (Figure 1). During the next 24 hours the depression started to fill and its central pressure increased gradually. By 0000 UTC on 5 March, while the Siberian high-pressure propagated westward, the

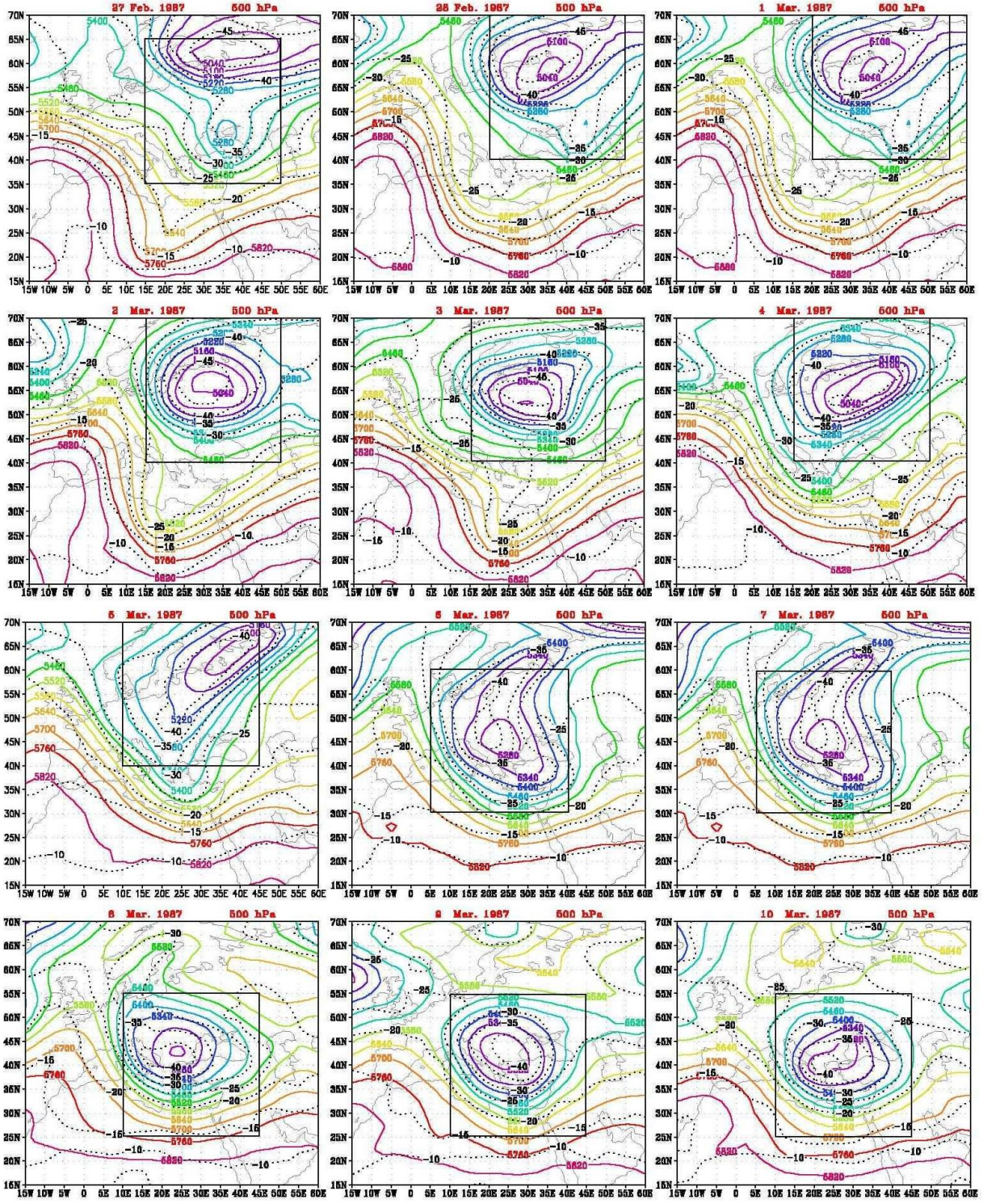

Fig. 1. 500 hPa height contours in 60 m intervals (solid) and temperature (dashed) in 5C increments for 0000 UTC 27 Feb. to 10 Mar. 1987. The closed boxes show the computational domain at each day.

horizontal extension of the cyclone decreased and slowly moved eastward. The 6-10 March period (Figure 1) was characterized by a Siberian anticyclone blocking, which started over Europe and became a stationary vortex rotating above the north east of Mediterranean. This type of the Mediterranean low is called a composite Cyprus low (EL-Fandy, 1946). Finally, the cyclone drifted slowly northeastward and was out of the computational domain by 11 March.

2. Data and Methodology

2.1 Data

2.1.1 CMWF data

Meteorological data used in this study were taken from the archives of the European Center for Medium Range Forecasting (ECMWF). These data comprise the horizontal wind components (u-eastward, v-northward), the temperature (T) and the geopotential height (z) on regular latitude-longitude grid points with $2.5^o \times 2.5^o$ resolution. The data are available only at 0000 UTC the 27 February to 10 March period for isobaric levels 1000, 850, 700, 500, 400, 300, 250, 200, 150 and 100 hPa. The domain of the study extended from 15.0^o to 70.0^oN and from 15.0^oW to 60.0^oE. The inner domain used in the present study changes with time to enclose the cyclone under investigation (see Figure 1).

2.1.2 Total ozone data

This study used total Ozone Mapping Spectrometer (TOMS) data measured by the Nimbus 7 satellite. Daily data for the 1978-1988 period were obtained on CD-R from the National Space Science Data Center (NSSDC) in the United States. Version 6 TOMS data, corrected for a negative drift due to the degradation in the reflectivity of the aluminum diffuser plate on the TOMS instrument. Data resolution is 1^o latitude by 1.25^o longitude. The data are measured in Dobson Units (DU), where 1000 DU are equivalent to 1 cm of ozone at 1000 hPa.

2.1.3 Ozone Profile data

Ozone profile data were obtained from the Solar Backscatter Ultraviolet (SBUV) instrument onboard the Nimbus 7 spacecraft. Data covering the entire Nimbus 7 SBUV lifetime, November 1, 1978 through June 21, 1990, are given as daily files of individual measurements, and as zonal means. The Nimbus 7 spacecraft was in a south-to-north, sun-synchronous polar orbit so that it was always close to local noon/midnight below the spacecraft. Thus, ozone measurements were taken every 24 hours for the entire planet. SBUV has nadir-viewing instruments with a 200 kilometer square field of view at the sub-satellite point. One measurement is made every 32 seconds along the orbital track, approximately every 1.8 degrees in latitude, from 80 degrees south to 80 degrees north. SBUV directly measures the ultraviolet scattered by the earth's atmosphere at 12 wavelengths, from 255 nm to 340 nm. The vertical ozone profile inversion is done in Umkehr layers ($\sim$ 5 km thick layers) although the actual vertical resolution of the SBUV instrument is approximately 8 km in the upper stratosphere and drops significantly in the lower stratosphere as a result of broader low-level contribution functions and multiple scattering contamination.

2.1.4 Method of analysis

The occurrence of an anomalous high potential vorticity value reaching down towards middle tropospheric height levels is a key indicator of a fold like ingress of stratospheric air into the troposphere. Hence, potential vorticity fields were calculated from the available meteorological parameters, namely temperature, and the horizontal wind components on constant pressure surface.

In isobaric coordinates the potential vorticity was approximated by the product of the vertical components of absolute vorticity and potential temperature gradient as

$$PV = -\left[\left(\frac{\partial v}{\partial x} - \frac{\partial u}{\partial y}\right) + f + \frac{R}{\sigma P}\left(\frac{\partial v}{\partial p}\frac{\partial T}{\partial x} - \frac{\partial u}{\partial P}\frac{\partial T}{\partial y}\right)\right]_p \frac{\partial \theta}{\partial p}, \tag{1}$$

where f is the Coriolis parameter, θ is the potential temperature, u and v are the velocity components in the x and y directions respectively. Following WMO (1986) the dynamic tropopause is defined by the potential vorticity with $PV = 1.6 \times 10^{-6}$ Kpa^{-1} s^{-1} = 1.6PVU.

For the present study, a useful property of a Q-vector field is the approximate proportionality of its divergence to the negative vertical velocity in a quasi-geostrophic approximation on an f-plane (Hoskins *et al.*, 1978). In isobaric coordinates this proportionality results in $\nabla_p \dot{Q} \sim \omega$, where $\omega = dp/dt$. This result lead to the finding of that a promising additional analysis tool for diagnosing the presence of tropopause folds with downward motions can be based on the divergence of Q-vectors. Following Holton (1992), patterns of Q-vector divergences can be observed in the vicinity of troughs where adescend in the regions of cold air advection west of the trough and an ascend in the warm air advection regions east of the trough are expected.

Average total ozone was estimated by calculating the average gridded ozone values inside a closed box every day (see Figure 1). This closed box enclosed the cyclone cell over each day of the study, where the calculations of total ozone average and meteorological parameters were only made over this box. Also, the same procedure was applied to estimate the average vertical profile of ozone from Nimbus 7 SBUV data. The daily mean tropopause pressure values were taken over the fixed domain from NOAA - GAES climate diagnostics contour.

Centered finite differences were used to compute horizontal derivatives and all vertical derivatives except those at 1000 and 100 hPa, where forward and backward differences were respectively employed. The vertical motion, ω, is computed using the Q-vector representation of the quasi-geostrophic ω equation (Bluestein, 1992).

3. Horizontal distribution of potential vorticity and cyclogenesis

The evolution of the meteorological situations can also be illustrated by displaying a sequence of PV maps on the 300 hPa isobaric surface from 0000 UTC on 27 February to 0000 UTC on 10 March (Figure 2). The PV contour (line 1.6 PVU) can be thought to represent the boundary between tropospheric and stratospheric air.

On 27 February a very pronounced southward penetration of the PV contours was observed where a local maximum of PV of the stratospheric intrusion (65° N, 25° E) was found with a value greater than 5 PVU directly above the relative minimum in the 500 hPa geopotential height (Figure 1). The maximum of PV is an indication of the position of a deep tropopause. On 28 February a region with high $PV(>$ 3PVU) is related to a low-pressure system, which developed over the east Baltic sea with the associated upper air trough and a strong jet streak on the eastern flank of the low. On March the PV anomaly becomes more elongated, extending to the coast of North Africa as the jet streak moved into the trough of the baroclinic wave.

In the present case study, it seems that the PV anomaly at the upper levels is important for the initiation of surface cyclogenesis, as Hoskins and Berrisford (1988) claimed. In particular, the role of a PV anomaly is to maintain the dynamic instability at the upper levels (McWilliams, 1980), while it intensifies when advancing over a region of pre-existing baroclinicity (Reed *et al.*, 1992). The PV anomaly could interact with the low level baroclinic zone, in the way that Thorncroft *et al.*, (1993) suggested for frontal cyclogenesis. Since, according to Hoskins *et al.*, (1985), the appearance

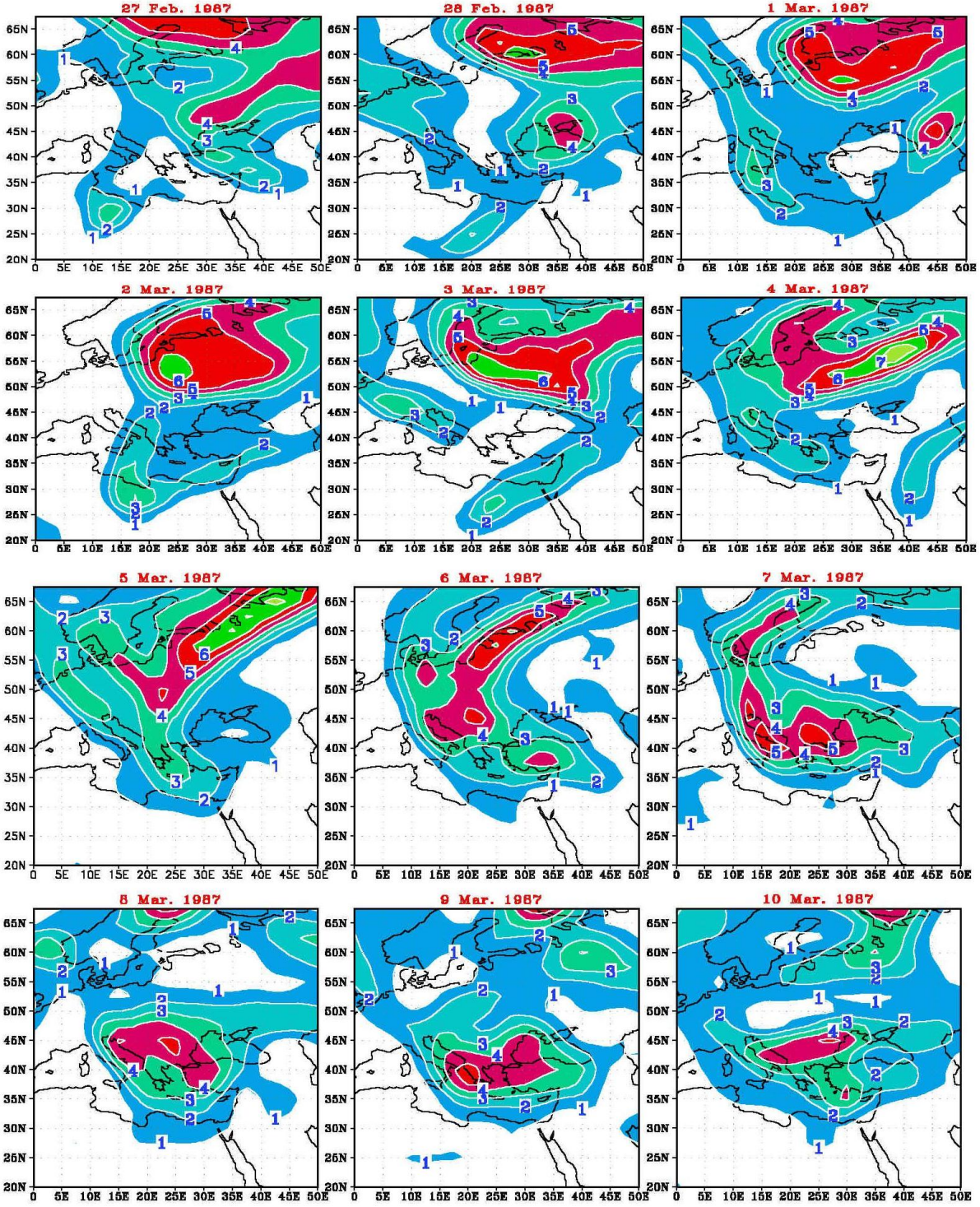

Fig. 2. Ertel potential vorticity on 300 hPa for the period 27 Feb. to 10 Mar. 1987. Potential vorticity units (PVU): 1PVU=10-6 M2 K Kg-1 S-1.

of the cut-off low at 500 hPa determines the termination of the dynamic supply to the low levels, surface factors seem to act primarily on the subsequent stages of this case of cyclogenesis.

On 2 March a maximum of PV on the western side of the stratospheric intrusion (55°N, 25°E) was observed with a value larger than 6 PVU directly above the relative minimum in the 500 hPa geopotential height (Figure 1). This main core of the PV trough propagates southwestward involving advection on its southern edge. On 3 March, the PV maximum had moved southeast, following the path of the upper-level and increased in values. Also, the $PV = 2$ PVU contour moved southeast to reach the southeast of the Mediterranean. On 4 March the maximum values of PV increased significantly (> 6PVU) and moved eastward. On 5 and 6 March the slow moving ridge of the Siberian high began to build westward, and so the horizontal extension of the cyclone decreased and moved slowly southeastward. This situation is clear because of the movement of the center of the high PV values where the 4 PVU value reaches the north boundary of the Mediterranean. The8-10 March period (Figure 2) was characterized by a Siberian anticyclone blocking that covered Europe, and the cyclone became a stationary vortex rotating above the northeast of the Mediterranean. Therefore, it is clear that the center of maximum decreased PV moved south to the northeast of the Mediterranean, following the low pressure center.

4. The correlation between ozone and potential vorticity

Danielsen (1968) demonstrated that there is a good correlation between the ozone mixing ratio and potential vorticity. He used this correlation to identify intrusions of stratospheric air into the troposphere for a limited geographical region. In a later study, this author (1985) showed that this correlation also holds for integrated time and longitude values on a hemispheric scale. The good correlation between total ozone and potential vorticity is plausible because the variation in both these quantities are transport dominated, both have high values in the stratosphere and low values in the troposphere. Figure 3 shows the values of total ozone during the life cycle of the case study. Comparing the behavior of total ozone (Figure 3) with the corresponding PV (Figure 2) during the period of study, it is clear that the centers of high values of PV are associated with the centers of ozone maximum.

In this study of the variation of the PV area average at each pressure level with the corresponding averages at the first five layers of ozone was investigated the column integrated PV for the same area and its correlation with the column integrated ozone (total ozone) is also estimated. Figures 4 and 5 show the time height variation of total ozone on the first five layers and the total PV at the pressure levels. Systematic changes, related to the life cycle of each case occur in the time height pattern of total ozone and PV (Figures 4 and 5). The major feature in these figures is the persistence of maximum values of ozone in layers L3 and L4 and above 300 hPa for PV. It is interesting to note that during the growth period the values of ozone increased and extended downward to reach its maximum (115 DU) between the layers L2 and L4 on 4 March. Also a large increase of PV during the period of growth occured and extended to the lower layers. During the decay period the total values of ozone and PV decreased.

Figure 6 shows the area average of integrated values of PV and total ozone amount over the enclosed domain. Clear positive correlation between the values of PV and ozone amount is seen where the correlation coefficient (r) between the two variables is calculated and is equal to 0.85.

5. Selected folding period

This section is concerned with the study of PV in relation to the polar jet stream trough system during the period from 1 to 6 March, where the maximum development of the cyclone occurred. A vertical cross-section was taken on each day of the selected period along the latitude where

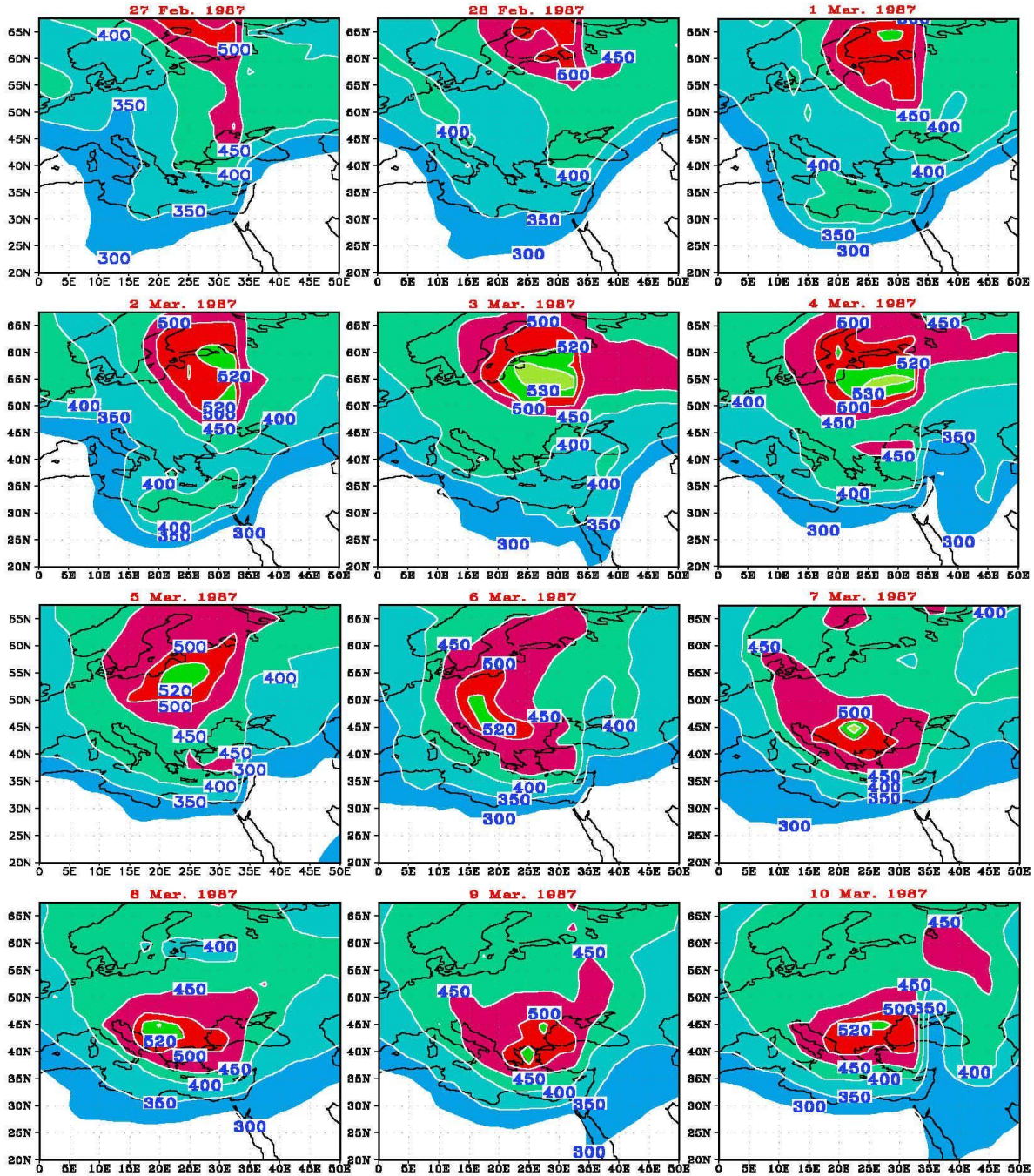

Fig. 3. Vertically integrated values of total ozone during the period 27 Feb. to 10 Mar. 1987.

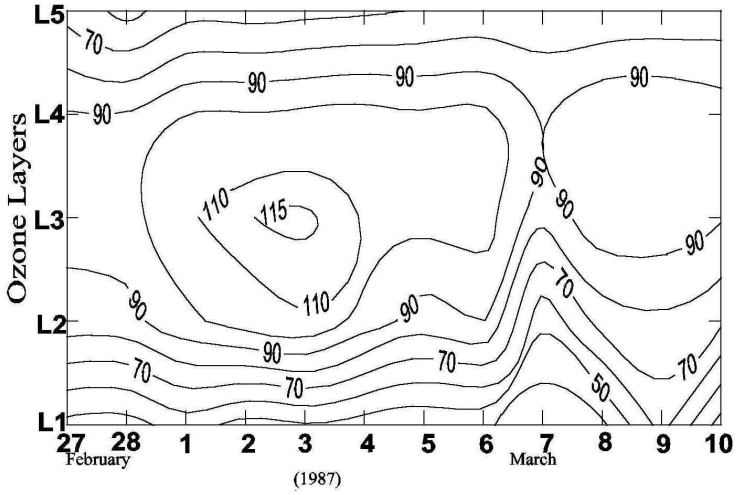

Fig. 4. Time height cross section of the area average values of ozone at the first five layers for the period 27 Feb. to 10 Mar. 1987.

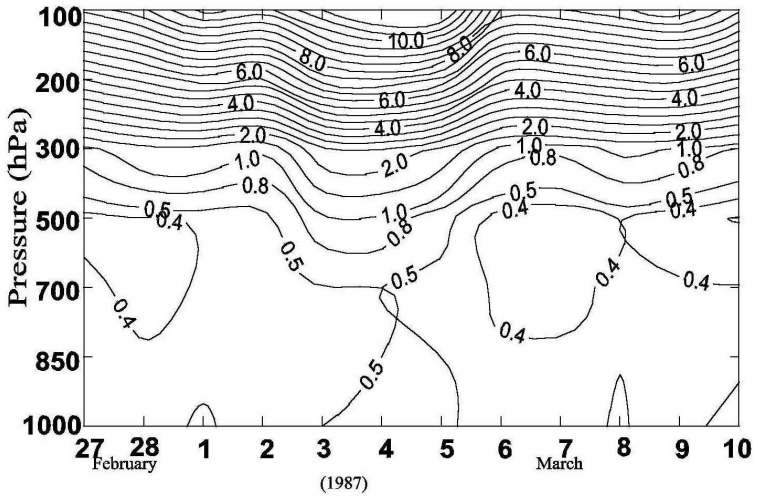

Fig. 5. Time height cross section of the area average potential vorticity values for the period 27 Feb. to 10 Mar. 1987

maximum PV exists. The selected latitude is listed above each figure representing the relevant day.

5.1 Vertical structure of PV and θ

A vertical cross-section of PV and q was taken to demonstrate the vertical structure and the anomalies at both upper and lower levels (Figure 7). The potential temperature field shows an upper level front, extending from 400 hPa, sloping from northeast to southwest. Associated with this upper level front, air with high potential vorticity stretched downward from the lower stratosphere into the mid-troposphere. The 1.6 PUV contour of potential vorticity that indicates the approximate position of the tropopause is marked. The upper level front appeared strong during the first three days (1, 2, and 3 March), and it weakened in the last days. The movement and downward extending of the 1.6 PUV contour is consistent with the movement and strengthening of the cyclone during the selected period. Figure 7 shows the movement of the PV maximum dur-

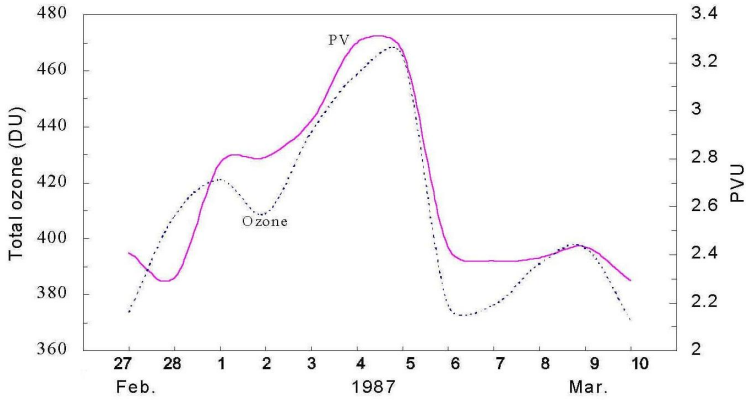

Fig. 6. The area average integrated values of potential vorticity with the corresponding of total ozone for the period 27 Feb. to 10 Mar. 1987.

ing the period of interest, where at 0000 UTC on 1 March a large maximum value of PV is located near 30°E. This maximum oscillates east-west and is associated to the movement of the cyclone. By 0000 UTC on 4 March, high PV values extend through the troposphere near 40°E, and a large region of low PV is apparently downstream, associated with the strong upper level ridge. By 0000 UTC on 6 March, the upper level system has practically cut off, and low level baroclinicity was weakened.

5.2 Vertical structure of PV and wind speed

Another perspective of PV evolution is provided in Figure 8, where cross-sections of PV and the total wind for the same time as in Figure 7 are shown. Along the period of interest it is clear that two centers of maximum wind appear, the first on the right side of the downward extension of PV (ahead of the PV maximum), and the second on the left side (behind the PV maximum). These two centers of maximum wind represent the core of the polar jets trough system. The east-west oscillation of the polar jets trough system is also associated to the movement of the downward extension of PV. It is interesting to note that the core of the polar jet associated to the west of the trough is greater than that associated to the east of the trough during the first three days (1, 2, and 3 March), while the inverse is satisfied on the last three days. Finally, the propagation of the intensifying polar jet through the short-wave trough is consistent with the "asymmetrical" thermal structure of upper level troughs preceding cyclogenesis as described by Palmen and Newton (1969, pp. 335-338).

5.3 Vertical structure of PV and ω

In order to understand the link between PV and vertical motion the quasigeostrophic vorticity equation in pressure coordinates was considered. Suppose that in the reference frame of the positive PV anomaly, geostrophic absolute vorticity does not change, even below where the induced wind field extends. Then

$$0 = -V_g \dot{\nabla}_p(\zeta_g + f) - \delta f_0. \tag{2}$$

The region west of the PV anomaly is located downstream from the induced cyclonic vortex in the moving reference frame. The vorticity advection is cyclonic there at low levels $[-V_g \dot{\nabla}_p(\zeta_g + f > 0]$, and hence the conclusion from equation (2) is that there must be a horizontal divergence ($\delta > 0$); similarly, upstream from the induced cyclonic vortex there is anticyclonic vorticity advection, and

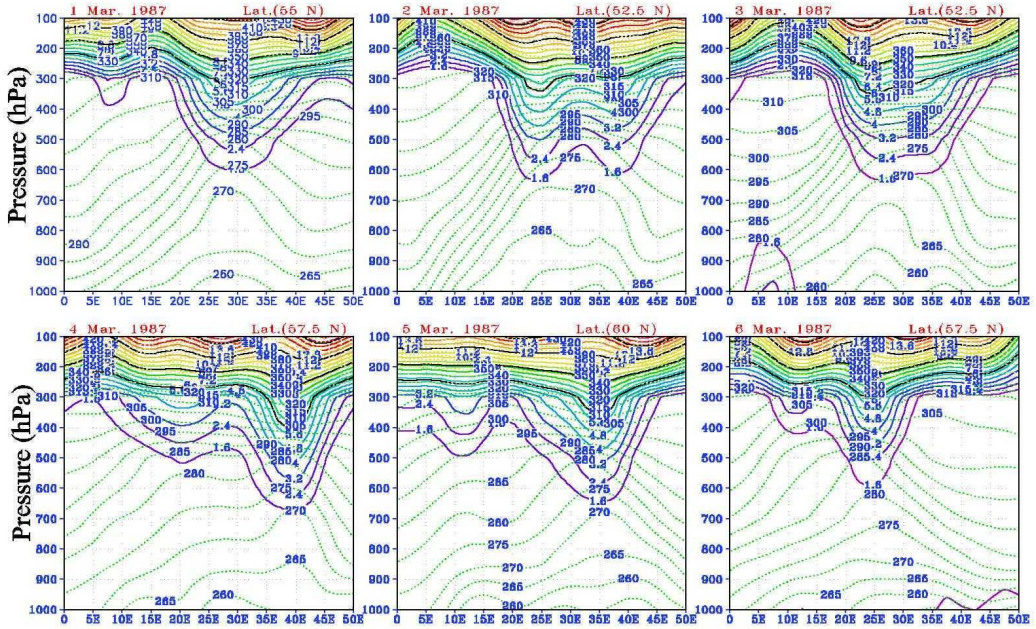

Fig. 7. Vertical cross section of potential vorticity in PVU (solid) and potential temperature in K (dotted).

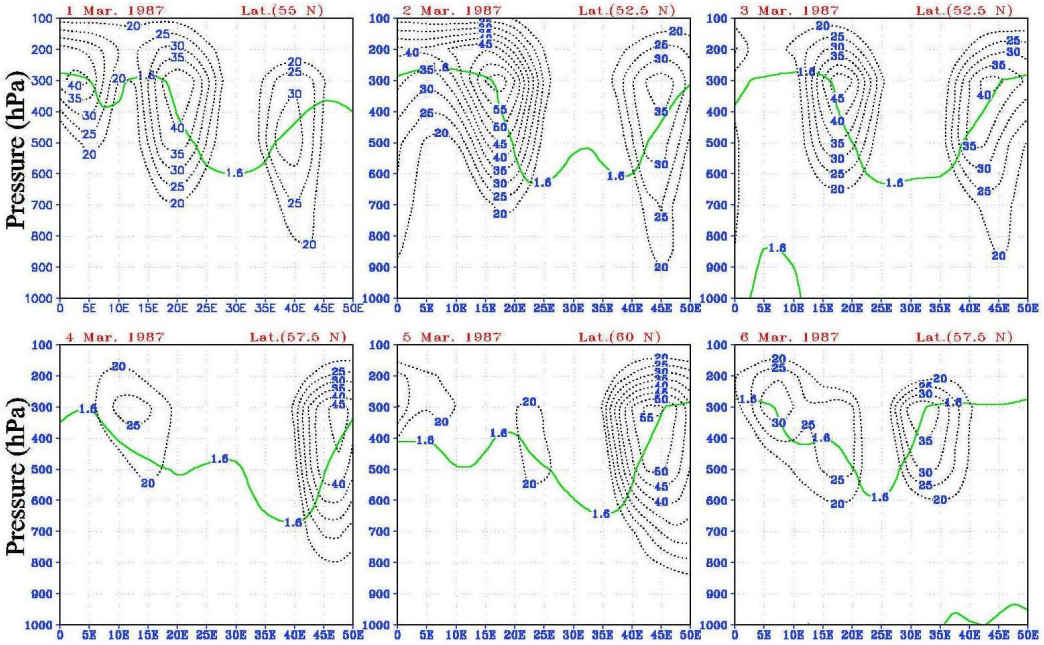

Fig. 8. Vertical cross section of the wind (dotted) and the contour of the dynamical tropopause (solid).The isotaches are every 5 m/s for the values 20 m/s.

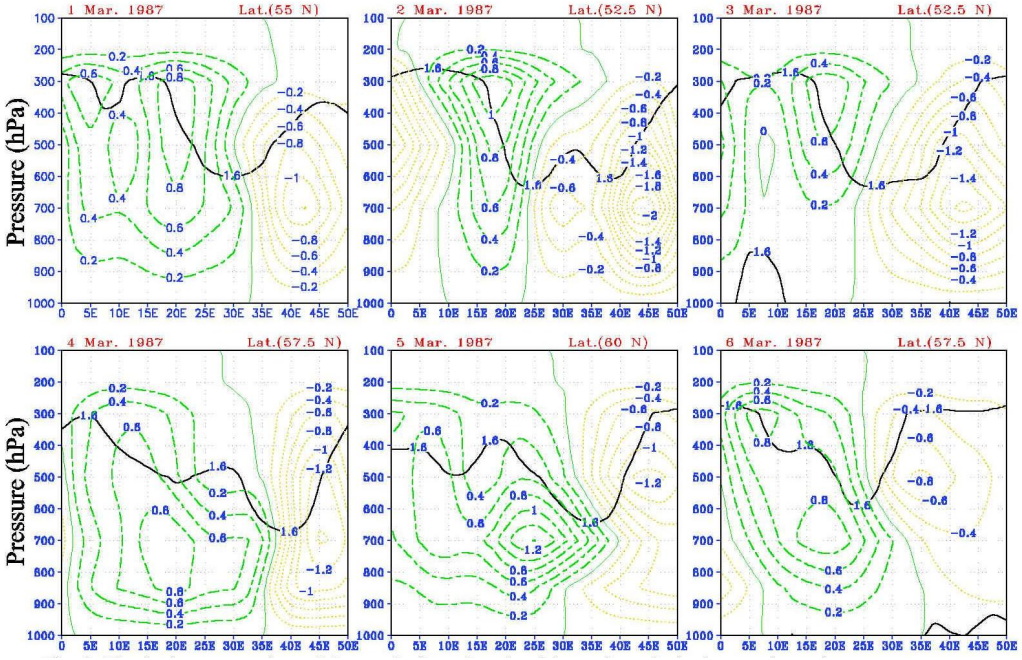

Fig. 9. Vertical cross section of the vertical motion (positive values dashed, negative values dotted) and the contour of the dynamical tropopause (solid).

convergence. Assuming that $\omega = 0$ at the ground level, the continuity equation can be used to deduce a rising motion east of the PV anomaly, and a sinking motion west of the PV anomaly.

A similar analysis of the vertical-motion field can be done using the adiabatic form of the thermodynamic equation. In the reference frame of the PV anomaly, $\partial T/\partial t = 0$, so that

$$0 = -V_g \dot{\nabla}_p T + \omega\sigma(P/R). \tag{3}$$

Below the positive anomaly the air is relatively cool. Therefore in the refrence frame of the eastward moving anomaly, below the anomaly, there is warm advection ($-V_g \cdot \nabla_p T > 0$) to the east, and cold advection to the west. From equation (3) it was deduced that if the atmosphere is statically stable there must be rising motion ($\omega < 0$) to the east and sinking motion ($\omega > 0$) to the west.

Figure 9 shows the cross-sections of ω and PV. It is important to note that west of the PV anomaly (downward extension of maximum PV), which is the area of cold air advection, there is a region of downward motion and east of the PV anomaly (the area of warm air advection) there is a dominant region of upward motion. Therefore, we can say that warm advection is usually associated to rising motion, and cold advection is usually associated to sinking motion. Since day to day variations of ω and PV were of key interest, two main features may be drawn from Figure 8 for the selected period: there is an upward motion west of the PV anomaly and a downward motion east of the PV anomaly. The centers of these vertical motions intensify and move along the cyclone.

5.4 Vertical structure of PV and $\nabla \cdot Q$

Following Sanders and Hoskins (1990), Q vectors are studied by considering the vector change in the geostrophic wind along an isotherm and rotating it anticyclonically through 90°. Figure 10

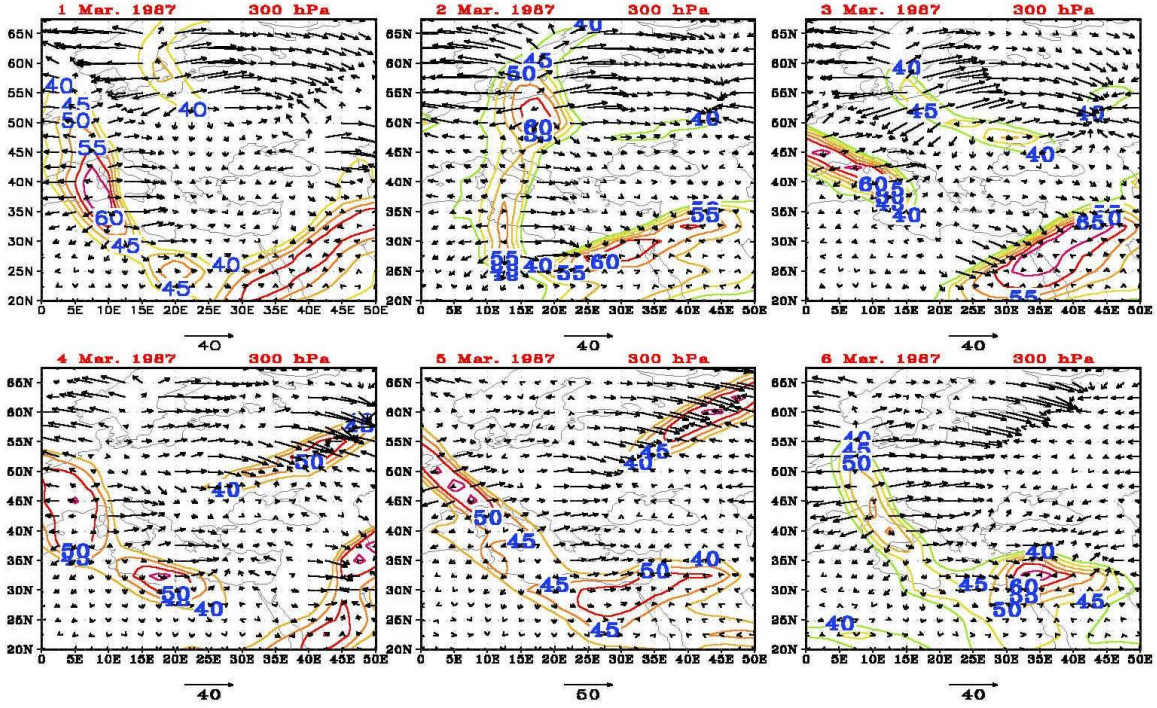

Fig. 10. Vector representation of the Q- vector field in the vicinity of the jet streams at 300 hPa for the selected period, overplotted with the contours of the jet streams greater than 40 m/s.

displays the Q vectors for the jet streak on the selected period. The direction of the arrows at both ends is away from the jet core, taking into account confluence and diffluence. The shortest length of the Q vectors is found in the middle region of the jet core where there is no confluence or shear in the horizontal wind: the length reflects the tendency to increase the temperature gradient in the cold frontal region. Figure 10 shows the Q vectors pointing in the direction of the low-level ageostrophic motion and towards the rising motion for the exit and entrance regions of the jet streak. This is consistent with the obtained transversal ageostrophic motion and with theoretical expectation. The Q-vector divergence/convergence inferred from Figure 10 illustrates the direction of vertical motion in the atmosphere around the jet streak at 300 hPa, with descent along the whole length of the jet streak, and ascent in the region at the jet entrance and at the jet exit. The sharpest descent is found in the exit and entrance regions, in agreement with the analyses of the tropopause folding. In the entrance region, the divergence of the Q-vector (and therefore descent) in the cold-front region is in agreement with the Q-vector analyses of a middle-latitude synoptic development, by Hoskins and Pedder(1980).

The vigorous system near the jet-exit area with large magnitude Q vectors relates to the developing vortex, with the direction of the Q vectors following approximately the curvature of the isentropes in that area. Also, the Q-vector field indicates descent to the west and ascent to the east of the developing cut-off low (COL) system (Figures 10 and 11) at 300 hPa. Finally, the strong divergence in the Q-vector field west of the developing COL, south of the jet exit, corresponds to an area where the tropopause folding can be resolved (Figures 10 and 11). This suggests that the circulation of the developing vortex may be significant in the extension of the folding beyond the jet exit and round the base of the COL.

In accordance with the theoretical foundations (Holton, 1992), the mesoscale simulations of the four episodes show that particularly high values of $\nabla\dot{Q}$ are restricted to regions of frontogenetic

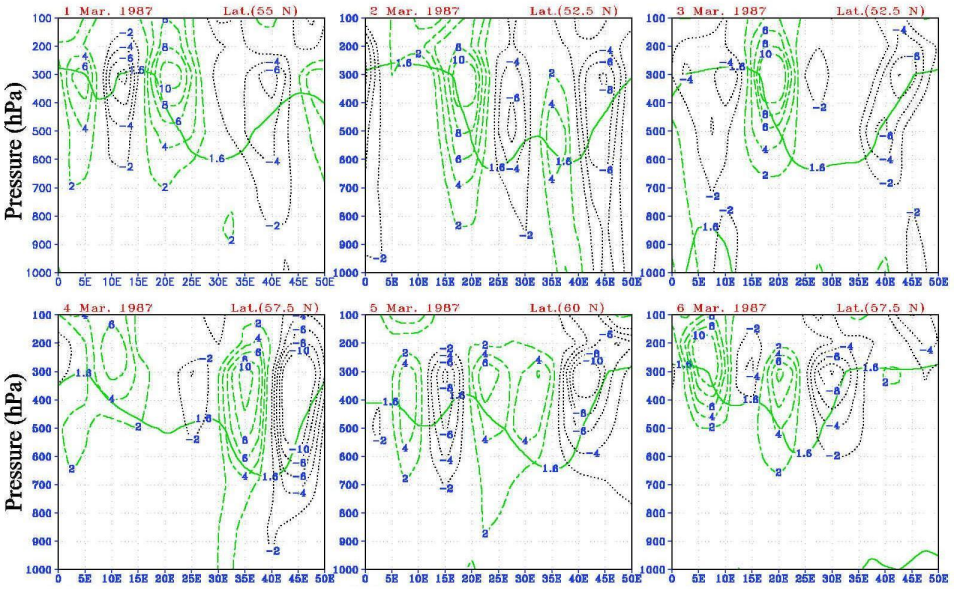

Fig. 11. Vertical cross section of .Q (positive values dashed, negative values dotted) and the contour of the dynamical tropopause (solid).

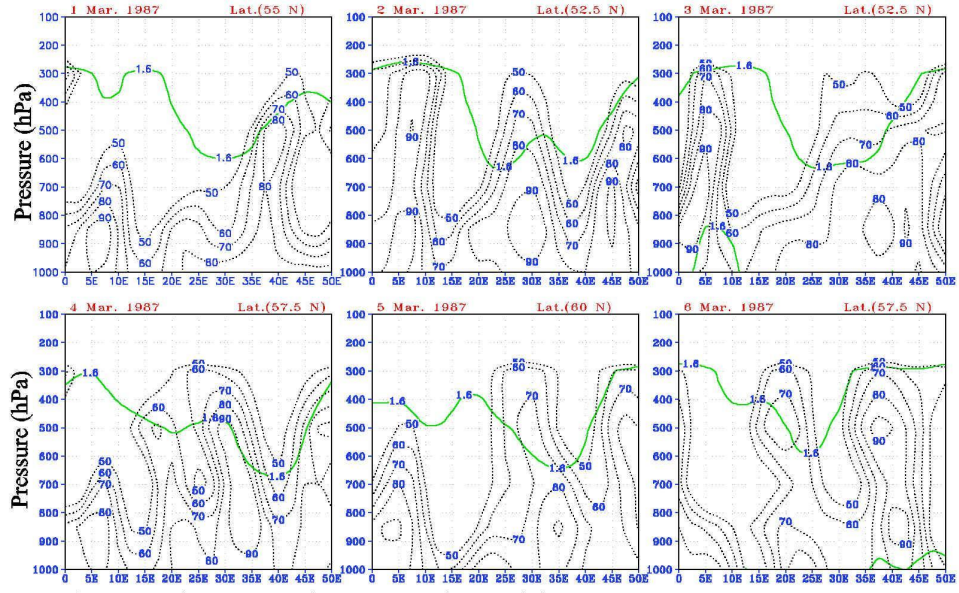

Fig. 12. Vertical cross section of the relative humidity (dotted) and the contour of the dynamical tropopause (solid).

activity. Consequently, extraordinary high values of $\nabla\dot{Q}$ can be directly related to frontogenesis.

On all days of the selected period the 400 hPa level as well as the 500 hPa level show horizontal maxima of $\nabla\dot{Q}$ (Figure 11). On most days $\nabla\dot{Q}$ was maximal, either at 400 hPa or at 500 hPa, and a potential vorticity undulation was clearly recognizable as a relative maximum of the PV at the 400 hPa level. Therefore, tropopause foldings may be reliably identified with the aid of the 400 to 500 hPa layer by potential vorticity maxima together with $\nabla \cdot Q$ maxima.

Figures 11 and 12 show the cross-sections of $\nabla\dot{Q}$ and relative humidity (RH). It is intersting to note that the area of negative $\nabla\dot{Q}$ (which is a region of upward motion) is associated to the area of maximum increasing and upward extension of RH. Also, the regions of positive $\nabla\dot{Q}$ are associated to regions of decreasing RH. his illustrates several aspects of the relationship between PV and water vapor. Generally at the base of upper troughs such as $PV = 2$ is concentrated on the warm side (dry area) and viceversa.

6. Conclusion

An analysis of a Mediterranean system during the period 27 February to 10 March, 1987 is presented. The study includes the investigation of the relation between total ozone and potential vorticity, as well as tropopause folding is associated to the polar jet (PJ). The most significant findings are the following:

(1) A strong correlation between total ozone and column integrated potential vorticity holds well on all levels. As both quantities are integrals through the atmosphere this result is consistent with, but does not prove, a high independent linear dependence between ozone and PV.
(2) The maximum movement of ozone from the stratosphere to the troposphere is coinciding with the maximum developing system, and also with the maximum values of PV.
(3) The amplification of the PJ- trough system occurred prior to cyclogenesis. The amplifying PJ- trough was first marked by a strong subsidence along the axis of the PJ between the trough and upstream ridge axes.
(4) A tropopause fold was associated to an intensifying PJ- trough system, and the formation of the fold was related to the subsidence forced by geostrophic deformation patterns connected with the jet streak.
(5) Q-vector diagnostics can still serve as a helpful tool for restricting the search to only one height level to distinguish between exchange free tropopause undulations and tropopause folds with subsequent mixing of stratospheric air into the troposphere.
(6) The Q-vector analysis also confirmed the position of the small folding along the jet and revealed a large-scale ascending motion that accounts for the small size of the folding. The Q-vector divergence maximum corresponds to a frontogenetically induced subsiding vertical motion and its strength is used to rate the activity of the folding.
(7) The scale-interactive dynamically forced vertical circulation played an important role in the extrusion of stratospheric air along the axis of a polar jet and the overall development of the storm system.

Acknowledgements

The authors would like to acknowledge the continuous support and encouragement of Prof. T.N. Krishnamurti.

References

Ancellet, G., J. Pelon, M. Beekmann, A. Papayannis, and G. Megie, 1991. Ground-based lidar studies of ozone exchanges between the stratosphere and the troposphere. *J. Geophys. Res.*, **96**, 22, 401 - 22, 421.

Ancellet, G., M. Beekmann and A. Papayannis, 1994. Impact of a cut off low development on downward transport of ozone in the troposphere. *J. Geophys. Res.*, **99**, 3451-3468.

Appenzeller, C. and H. C. Davies, 1992. Structure of stratospheric intrusions into the troposphere, *Nature*, **358**, 570.

Appenzeller, C., H. C. Davies and W. A. Norton, 1996. Fragmentation of stratospheric intrusions. *J. Geophys. Res.*, **101**, 1435-1456.
Bluestein, H., 1992. Synoptic-Dynamic Meteorology in Midlatitudes V.I. Principles of Kinematics and Dynamics. *Academic Press*, New York.
Browell, E., E. Danielsen, S. Ismail, G. L. Gregory and S. M. Beck, 1987. Tropopause fold structure determined from airborne lidar and in situ measurements. *J. Geophys. Res.*, **92**, 2112- 2120.
Danielsen, E. F., 1968. Stratospheric-Tropospheric Exchange based on Radioactivity, Ozone, and Potential Vorticity. *J. Atmos. Sci.*, **25**, 502-518.
Danielsen, E. F. and V. A. Mohnen, 1977. Project Dustorm report: Ozone transport, in situ measurements, and meteorological analyses of tropopause folding. *J. Geophys. Res.*, **82**, 5867-5877.
Danielsen, E. F. 1985. Ozone transport. Pp 123-160 in Ozone in the free atmosphere. Eds. R. C. Whitten and S. S. Prasad. Van Nostrand Reinhold.
Danielsen, E. F., S. Hipskind., W. L. Starr., J. F. Vedder., S. Gaines, and K. K. Kely, 1991. Irreversible transport in the stratosphere by internal waves of short vertical wavelength. *J. Geophys. Res.*, **96**, 17433-17452.
EL-Fandy, M. G., 1946. Baroclinic low Cyprus. *Q. J. R. Meteorol. Soc.*, 72, 291-306.
Holton, J. R., 1992. An Introduction to Dynamic Meteorology, 3rd edn. San Diego: Academic Press, 511 pp.
Hoskins, B. J. and F. P. Bretherton, 1972. Atmospheric frontogenesis models: Mathematical formulation and solution. *J. Atmos. Sci.*, **29**, 11-37.
Hoskins, B. J., I. Draghici, and H. C. Davies, 1978. A new look at the w- equation. *Q. J. R. Meteorol. Soc.*, **104**, 31-38.
Hoskins, B. J., and Pedder, M. A., 1980. The diagnosis of middle latitude synoptic development. *Q. J. R. Meteorol. Soc.*, **106**, 707-719.
Hoskins, B. J., M. E. McIntyre, and A. W. Robertson, 1985. On the use significance of isentropic potential vorticity maps. *Q. J. R. Meteorol. Soc.*, **111**, 323- 331.
Hoskins, B. J. and P. Berrisford, 1988. A potential vorticity prespective of the storm of 15- 16 October 1987. *Weather*, **43**, 122- 129.
McWilliams, J. C., 1980. An application of equivalent models to atmospheric blocking. *Dyn. Atmos. Oceans.*, 5, 43- 66.
Palmen, E., and C. W. Newton, 1969. Atmospheric circulation systems: Their structure and physical interpretation. International Geophysical Series, Academic Press, **13**, 603 pp.
Reed, R. J., 1955. A study of characteristic type of upper-level frontognesis. *J. Meteor.*, **12**, 226-237.
Reed, R. J. and F. Sanders, 1953. An investigation of the development of a mid-tropospheric frontal zone and its associated vorticity field. *J. Meteor.*, **10**, 338- 349.
Reed, R. J., M. Stoelinga, and Y- H. Kuo, 1992. A model-aided study of the origin and evolution of the anomalously high potential vorticity in the inner region of rapidly developing marine cyclone. *Mon. Wea. Rev.*, **120**, 893- 913.
Sanders, F. and B. J. Hoskins, 1990. An easy method for estimation of Q-vectors from weather maps. *Weather and forecasting*, **5**, 346- 353.
Shapiro, M. A., 1980. Turbulent mixing within tropopause folds as a mechanisum for the exchange of chemical constituents between the stratosphere and troposphere. *J. Atmos. Sci.*, **37**, 994-1004.
Thorncroft, C. D., B. J. Hoskins, and M. E. McIntyre, 1993. Two paradigms of baroclinic-wave lifecycle behaviour. *Q. J. R. Meteorol. Soc.*, **119**, 17-55.
WMO, 1986. Atmospheric ozone, Vol. I. Report No. 16. Geneva: WMO, 264 pp.